

Paterson, D. J., Tassieri, M. , Reboud, J. , Wilson, R. and Cooper, J. M. (2017) Lipid topology and electrostatic interactions underpin lytic activity of linear cationic antimicrobial peptides in membranes. *Proceedings of the National Academy of Sciences of the United States of America*, 114(40), E8324-E8332. (doi:[10.1073/pnas.1704489114](https://doi.org/10.1073/pnas.1704489114))

This is the author's final accepted version.

There may be differences between this version and the published version. You are advised to consult the publisher's version if you wish to cite from it.

<http://eprints.gla.ac.uk/145693/>

Deposited on: 26 September 2017

Enlighten – Research publications by members of the University of Glasgow
<http://eprints.gla.ac.uk>

Lipid topology and electrostatic interactions underpin lytic activity of linear cationic antimicrobial peptides in membranes.

David J. Paterson^a, Manlio Tassieri^a, Julien Reboud^a, Rab Wilson^a and Jonathan M. Cooper^{a,1}.

^aDivision of Biomedical Engineering, University of Glasgow, Rankine Building, Glasgow, G12 8LT, UK.

¹To whom correspondence should be addressed. E-mail: jon.cooper@glasgow.ac.uk

CLASSIFICATIONS: Biological Sciences/Chemistry; Physical Sciences/Engineering

KEYWORDS: Antimicrobial peptides; biomimetic; giant unilamellar vesicle; GUV; magainin; melittin; microfluidic; lipid; pore.

Linear cationic antimicrobial peptides are a diverse class of molecules that interact with a wide range of cell membranes. Many of these peptides disrupt membrane integrity by forming membrane-spanning pores, that ultimately lead to cell death. Despite their high potency and ability to evade acquired bacterial drug resistance, there is a lack of knowledge on their selectivity and activity mechanisms. Such an understanding would provide an informative framework for their rational design and could lead to novel antimicrobial therapeutic targets. In this paper, we use a novel high-throughput microfluidic platform as a quantitative screen to assess the peptides activity and selectivity by precisely controlling their exposure to vesicles with lipid compositions that mimic both bacterial and mammalian cell membranes. We explore the complexity of the lipid-peptide interactions governing membrane-disruptive behaviours and establish a link between peptide pore formation and lipid-peptide charge and topological interactions. We propose a novel topological model for linear antimicrobial peptide activity, based upon the increase in membrane strain due to the continuous adsorption of peptides to the target vesicle, coupled with the effects of both lipid-peptide charge and topographical interactions. We also demonstrate the validity of the proposed model by using two prototypical linear cationic peptides: magainin 2 amide (which is selective for bacterial cells) and melittin (which targets both mammalian and bacterial cells indiscriminately). Finally, we propose the existence of a negative feedback mechanism that governs the pore-formation process, and controls the membrane's apparent permeability.

Significance statement

We propose a new mechanistic framework that explains the activity and selectivity of an important class of compounds, known as linear cationic antimicrobial peptides. These molecules have the potential to be developed into highly potent and selective pharmaceuticals as they are able to discriminate between disrupting mammalian and bacterial membranes. By comparing both selective and non-selective peptides, we show that peptide activity is governed by topological and electrostatic interactions between the membrane-bound peptide and the surrounding lipids. This framework could underpin novel strategies for the rational design of new therapeutic agents that are potentially able to bypass the mechanisms of acquired bacterial drug resistance.

Introduction

The emergence of drug-resistant bacteria presents a pressing challenge to medicine.^[1-2] New therapeutic compounds are needed to break the cycle of resistance that occurs after the introduction of new antibiotics.^[3-4] Linear cationic antimicrobial peptides (LCAMPs) are potential antibiotic candidates, with many of them showing high potency against gram-negative and gram-positive bacteria at low micromolar concentrations.^[5] They are particularly interesting as they are immune from bacterial drug-resistance mechanisms.^[5-6] The class of LCAMPs are diverse, with over 1,000 members

expressed in widely separated taxonomic groups; characterized by their amphipathic and cationic membrane-bound helices.^[7-9] Unlike most peptide families, it is the physiochemical properties of the LCAMPs' assembled helices which renders them homologous, rather than their amino acid sequence.^[10-11] Some LCAMPs are selective for bacterial cells, e.g. magainin 2 amide (m2a) from the African clawed frog *Xenopus laevis*.^[8] Others target bacterial and mammalian cells indiscriminately, e.g. melittin, the from the venom of the bee *Apis mellifera*.^[9]

Although many complex lipid-peptide interactions, involving e.g. electrostatics and peptide hydrophobic moments have been proposed to influence their behavior,^[12-13] a full understanding of the relationship between LCAMPs and the cell's membrane is not complete.^[6-7] One mechanism widely used to describe LCAMP behavior is the Shai-Matsuzaki-Huang (SMH) model, shown in Fig. 1A to E.^{[6][15]} Briefly, LCAMPs display random-coil conformations in aqueous environments, before spontaneously binding to lipid bilayers, where they adopt an amphipathic helical configuration. The peptides initially insert parallel to the membrane plane, leading to membrane thinning, as LCAMP helices increase their outer leaflet volume.^{[7-8][15]} Once a threshold concentration of membrane-bound peptide has been achieved, membrane integrity becomes compromised through a variety of peptide-induced effects (PIEs) including: bursting, a detergent-like carpet mechanism, and formation of membrane spanning toroidal pores.^{[7][9][16][17]} The latter is marked by a shift in

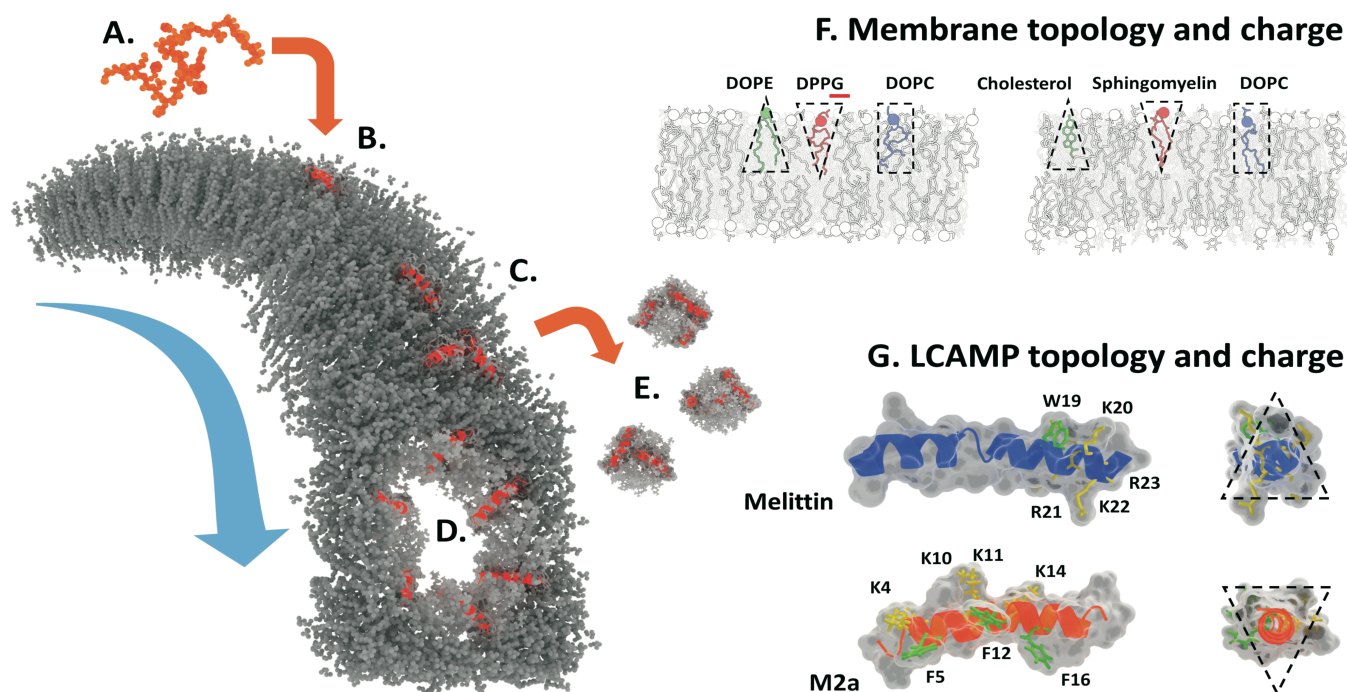


Fig. 1: The Shai–Matsuzaki–Huang model of LCAMP activity in lipid bilayers (grey). (A) LCAMPs (orange) bind to the outer membrane leaflet as amphipathic helices (B). Membrane-bound peptides (C) produce a variety of effects, including toroidal pore formation (D) and the release of lipid-peptide micelles in a detergent-like carpet mechanism (E). (F) Bacterial and mammalian membranes are characteristically different in charge and lipid topology. Bacterial outer leaflets contain lipids with large anionic headgroups (e.g. DPPG), and conical non-bilayer lipids (e.g. DOPE), giving them a negative net charge and curvature profile. Mammalian outer leaflets contain bilayer lipids like sphingomyelin, along with the conical geometry cholesterol, a lipid completely absent from bacterial membranes. They are net neutral in charge and curvature profile. (G) Similarly, melittin (blue) and m2a (orange) vary in charge and topological character. The four cationic lysines (K; yellow) and three phenylalanines (F; green) of m2a are distributed along its length, while the cationic arginines (R; yellow) and lysines (K; yellow) of melittin are clustered at the c-terminus, along with its single tryptophan residue (W; green). Melittin acts as a negative curvature membrane wedge (conical geometry), while m2a acts as a positive curvature wedge (inverse-conical geometry).

helical orientation (from parallel to perpendicular to the membrane plane), and by translocation of lipid and peptide material from the outer to the inner membrane leaflet. Although the SMH model provides a basic mechanistic framework for LCAMP activity, it cannot predict peptide activity within specific membrane systems, e.g. it is not able to explain LCAMP selectivity between bacterial and mammalian membranes, which are characteristically different in both charge and topology (Fig. 1F).

Bacterial cells contain high proportions of anionic and conical geometry non-bilayer lipids, whereas the outer leaflets of mammalian membranes are zwitterionic with a neutral curvature profile.^[18-19] These marked differences in membrane charge and topology are reflected in the physiochemical properties of two LCAMPs, the selective m2a and the non-selective melittin (Figs. 1G and 2). The cationic residues of m2a are distributed along its length in close proximity to three sterically active phenylalanine residues, and form a large angle on the helical face.^[14] The wide polar angle renders m2a unable to fully insert into the hydrophobic core of lipid bilayers, acting as a membrane “wedge” that induces positive curvature.^[9-10] In contrast, melittin has a single sterically active tryptophan near its c-terminus, where it clusters with its cationic residues, with a narrow polar angle formed on its helical face.^{[7][14]} Melittin acts as a negative curvature-inducing membrane wedge, owing to the deep penetration of its helix into the lipid bilayer.^[20] We now demonstrate that these inherent differences in lipid and peptide charges and topologies underpin LCAMPs activity and their selectivity between mammalian and bacterial cells.

We use giant unilamellar vesicles (GUVs) as model systems of cell membranes. GUVs with different lipid topology and charge, but with comparable size and curvature to mammalian cells, are exposed to LCAMP within a high-throughput microfluidic device (Fig. S1A). Dye-leakage experiments are used for the investigation of lipid-peptide interactions,^{[21][22]} and we have previously used such a technique, within a microfluidic platform, to precisely control the exposure of GUVs to LCAMPs.^[23] An advantage of this approach is the greatly increased experimental throughput over conventional techniques, which typically study only one GUV at a time.

By generating extensive dye-leakage data sets, from over 1,500 GUVs with different lipid compositions, we are able to gain new insights into lipid-peptide topology and electrostatic interactions, that are consistent with the existing SMH model. In particular, we not only provide a mechanistic explanation of LCAMP activity and selectivity, but also a predictive framework for peptide action within specific membranes. We show that the diverse membrane-disruptive activity of LCAMPs can be explained both through the accumulation of membrane strain and the relationship between lipid and peptide shape and charge. This extended model describes, for the first time, the selectivity mechanism of m2a for bacterial over mammalian cells, as well as the non-selective nature of melittin.^[8-9] Finally, we propose a novel negative feedback mechanism within the pore-formation process, that controls the membranes apparent permeability.

Results

We describe the effects of lipid charge and topological character on overall LCAMP lipid clustering and activity, as well as the classification of peptide-induced effects (PIEs) and the dynamics of pore-mediated dye-leakage.

Activity: Overall LCAMP activity was determined by the relationship between peptide and lipid topology with m2a and melittin activity arising in systems with opposing lipid geometries (Table 1). Membrane-bound proteins form dynamic lipid rafts, shown to be capable of preferentially associating with specific lipids, including cholesterol and sphingolipids.^[24] Fig. 2 shows the expected lipid associations of both m2a and melittin, within all seven membrane compositions investigated (#A to #G), with consideration given to four factors, namely:

(i) Membrane curvature: this is a modulator of lipid and protein localization as membranes seek to minimize free energy through reduction of their internal packing strain.^[25-27] By considering the established ability of melittin and m2a to induce opposing curvature in similar membranes, the peptides minimize packing frustration around them by clustering with lipids opposing the peptide-induced curvature.^{[9][16][20]} For example, membrane systems #B and #C contain positive curvature lipids (DPPC) that oppose melittin's negative curvature induction: i.e. they lower raft energy by clustering around the peptide helix;

(ii) Aromatic interactions: It is known that cholesterol forms π -stacking interactions with tryptophan and phenylalanine residues.^{[28][29]} Here, cholesterol can cluster with phenylalanine residues of m2a, and the sole tryptophan of melittin. The aromatic interactions bring a negative curvature lipid into

contact with LCAMPs in the mammalian biomimetic membrane (System #A);

(iii) Electrostatic interactions: these are powerful mediators of lipid-LCAMP associations.^[12] For example, system #G contains the anionic lipid LPG, which will form clusters around the cationic residues of both peptides.

(iv) Residue distribution; the positioning of cationic and sterically bulky residues effects lipid distribution around the helix.^{[12][28][29]} M2a distributes these residues along its helical length and the lipids that associate with them (i.e. anionic lipids and cholesterol) will also locate along its helical length (Fig. 2). Melittin isolates these residues at the c-terminus, and anionic lipids and cholesterol will similarly locate there, leaving the helical face to associate with other lipid components.

These four factors underpin LCAMP activity, which we describe in more details in the following sections. Anionic lipids with low hydrophobic volumes and inverse-conical geometry will activate m2a. For example, membrane systems #C (DPPG), #F (DPPG) and #G (LPG) contain inverse-conical anionic lipids with saturated 16:0 palmitoyl fatty acids, and return activities of 49%, 72% and 51% respectively. Substituting DPPG with POPG (i.e. replacing a palmitoyl chain with an unsaturated 18:1; 9Z oleic chain) results in a fourfold decrease in activity between membrane #F (DPPG: 72%) and #E (POPG: 16%). Conversely, lipids with large hydrophobic volumes (e.g. DOPC, DOPE and DOPG), from their unsaturated 18:1 oleic fatty acid chains or cholesterol (a lipid with large negative curvature^[19]), inactivate m2a. Indeed, membranes #A (cholesterol), #B (DOPG) and #D (DOPG) return activities of 31%, 18% and 6% respectively. Similarly, within the context of topological constraints, melittin shows an

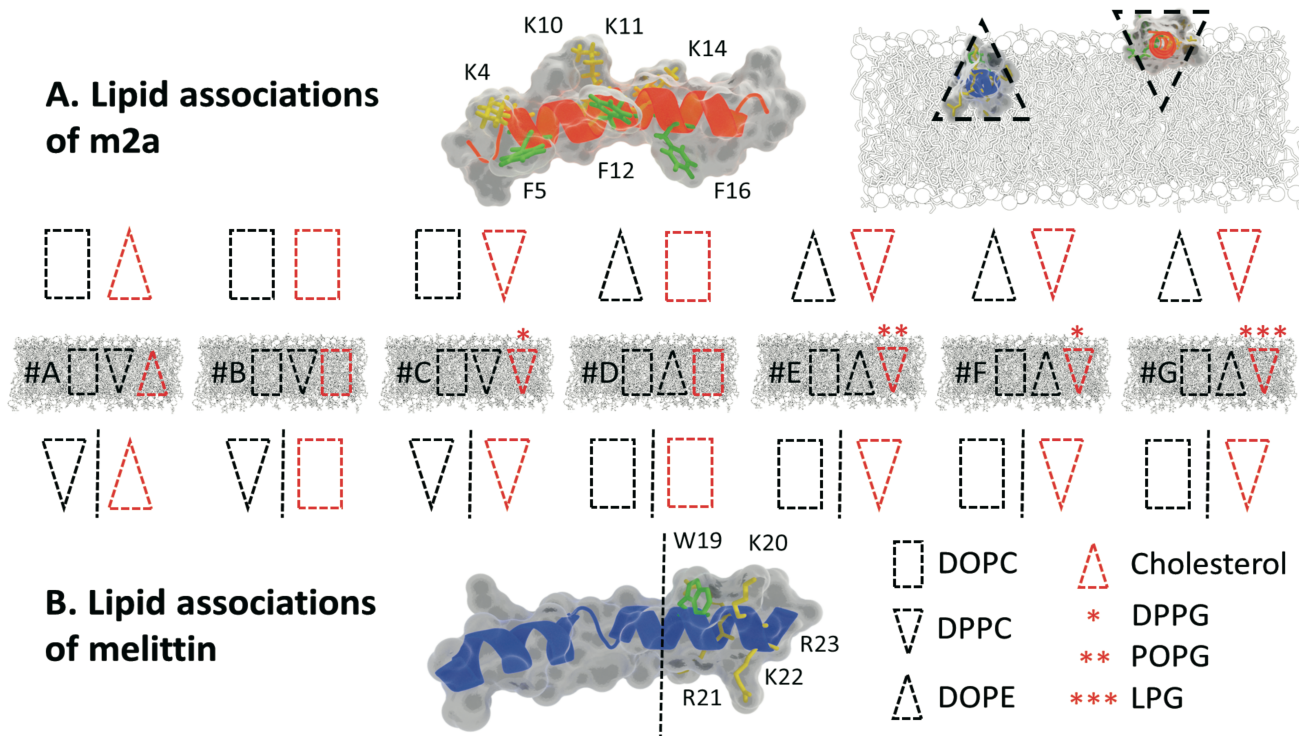


Fig. 2: The lipid associations of melittin and m2a, in the membrane systems #A to #G, with lipid topology indicated by the block shapes. A red outline indicates lipids with a clustering mechanism, either via electrostatics for the anionic lipids, or via aromatic π -stacking with phenylalanine (F) and tryptophan (W) for cholesterol. (A) The block shapes indicate the topology of the lipids expected to associate with m2a. (B) The lipid topologies expected to associate with melittin. Shapes to the left of the dashed line associate with the peptides helical face, while those to the right cluster with the peptides tryptophan and cationic residues at the c-terminus. (Inset, top right) The deeper penetration of melittin into the outer leaflet allows it to act as a negative curvature membrane wedge, while the shallower penetration of m2a results in a positive curvature wedge effect, indicated by the appropriate block shapes.

opposing trend compared to m2a. Its activity is enhanced by interaction with large hydrophobic volume lipids and reduced by the presence of inverse-conical low hydrophobic volume lipids. For instance, although melittin is generally more active than m2a, systems #C (DPPC and DPPG), #F (DPPG) and #G (LPG) show the highest activities for m2a, whereas they yield low melittin activities of 78%, 69% and 73%, respectively.

PIE classification. M2a and melittin behavior can be further classified into three groups: Pore-mediated leakage, where dye-efflux occurs with no loss of membrane volume;^{[7][16][17]} a detergent-like carpet mechanism, where dye-efflux is coupled to a loss of membrane volume;^{[7][9]} and bursting, where dye loss is complete and instantaneous (see also Figs. S4 to S8 and videos S1 to S3). Table 1 reports the percentage values of the PIEs recorded for the membrane systems #A to #G. It is clear that the two LCAMPs investigated vary widely in their membrane-disruptive behavior, even when tested using identical membranes. Below, we describe each of these leakage processes and build a correlation between them and their associated lipid-peptide interactions.

Pore events: The three highest levels of melittin pore activity occur in systems #A (37%); #B (58%) and #C (54%). Notably, they all contain the zwitterionic inverse-conical lipid DPPC, which is expected to cluster along the peptides helical face (Fig. 2). As LCAMP pore formation is coupled to a shift in peptide orientation, from parallel to the membrane plane to perpendicular to it,^{[15][17]} by inserting the center of the helix deep into the membrane core, it is likely that the pore rim is primarily composed of those lipids along the helical face. The opposite situation, where melittin clusters with high hydrophobic volume lipids along its helical face, i.e. DOPC in systems #D, #E, #F and #G, produces low levels of pore activity: 17%, 22%, 14% and 19%, respectively. Pore formation is therefore favored by the presence of positive curvature lipids, coupled to a clustering

mechanism that will enrich these lipids along the helical face. M2a displays high levels of pore formation in systems #C (38%) and #F (42%), where the peptide will cluster with the positive curvature anionic lipid DPPG, through electrostatic interactions with the cationic residues along the helical face. Membrane #C presents the highest relative pore formation of any lipid-peptide system tested, with 78% of active GUVs displaying pore-mediated leakage events.

Carpet events: Melittin displays a significant number of carpet events in systems #A (40%), #B (30%) and #D (47%); where it associates with high hydrophobic volume lipids at its c-terminus, either via electrostatic clustering with anionic conical geometry lipids, or via π -stacking interactions between tryptophan and cholesterol (Fig. 2).^{[12][28][29]} Conversely, our results (Table 1) show that carpet events are suppressed when melittin clusters with low hydrophobic volume lipids at its c-terminus; i.e. POPG in system #E (2%) and DPPG in systems #C and #F (10% and 13% respectively). M2a displays its highest levels of carpet events when clustered with lipids matching its own positive curvature induction, returning 15% in system #F (DPPG).

Bursting events: Melittin displays its highest levels of vesicle bursting in lipid compositions #D (33%), #E (43%) and #F (39%) where the peptide tends to form lipid rafts enriched with the high hydrophobic volume lipid DOPC. Conversely, bursting is suppressed when melittin associates with lipids having low hydrophobic volumes; i.e. DPPC in systems #A (22%), #B (3%) and #C (10%). M2a displays high levels of bursting in membranes where it forms rafts enriched with lipids having high hydrophobic volume; i.e. cholesterol and DOPC in membrane #A (18%), and DOPE in membranes #F and #G (12% and 28%, respectively). Bursting events are also strongly disfavored in system with composition #C, (no bursting activity, out of 59 GUVs observed), where m2a associates with

Table 1A. Peptide-induced effects of the LCAMP melittin

System #	Composition	No effect (%) ± SD	Pore (%) ± SD	Burst (%) ± SD	Carpet (%) ± SD	Other (%) ± SD
A	DOPC:DPPC:chol	0	37 ± 7	22 ± 4	40 ± 10	1 ± 2
B	DOPC:DPPC:DOPG	3 ± 4	58 ± 13	3 ± 3	30 ± 12	6 ± 7
C	DOPC:DPPC:DPPG	22 ± 13	54 ± 6	10 ± 6	10 ± 11	4 ± 4
D	DOPC:DOPE:DOPG	0	17 ± 12	33 ± 17	47 ± 8	2 ± 3
E	DOPC:DOPE:POPG	32 ± 12	22 ± 12	43 ± 14	2 ± 3	2 ± 3
F	DOPC:DOPE:DPPG	31 ± 12	14 ± 7	39 ± 10	13 ± 11	3 ± 6
G	DOPC:DOPE:LPG	27 ± 17	19 ± 2	27 ± 9	18 ± 7	9 ± 6

Table 1B. Peptide-induced effects of the LCAMP m2a

System #	Composition	No effect (%) ± SD	Pore (%) ± SD	Burst (%) ± SD	Carpet (%) ± SD	Other (%) ± SD
A	DOPC:DPPC:chol	69 ± 12	3 ± 5	18 ± 9	10 ± 6	1 ± 1
B	DOPCDPPC:DOPG	82 ± 6	7 ± 2	6 ± 5	0	6 ± 8
C	DOPC:DPPC:DPPG	51 ± 13	38 ± 11	0	7 ± 9	4 ± 3
D	DOPC:DOPE:DOPG	94 ± 6	0	3 ± 3	3 ± 3	0
E	DOPC:DOPE:POPG	84 ± 5	0	2 ± 5	9 ± 7	5 ± 10
F	DOPC:DOPE:DPPG	28 ± 12	42 ± 26	12 ± 12	15 ± 4	3 ± 4
G	DOPC:DOPE:LPG	49 ± 5	14 ± 3	28 ± 9	8 ± 14	0

PIEs of LCAMPs melittin (A) and m2a (B), in membrane systems #A to #G. Listed are the membrane compositions, the PIEs recorded for each lipid system after exposure to 1 μ M of the peptide, including no effect, pore-mediated leakage, carpet mechanism and other. Each data set is composed of at least 34 vesicles, from at least three independent experiments, and the standard deviation is included. Bolded values are the results discussed within the text, and are a guide to the eye only

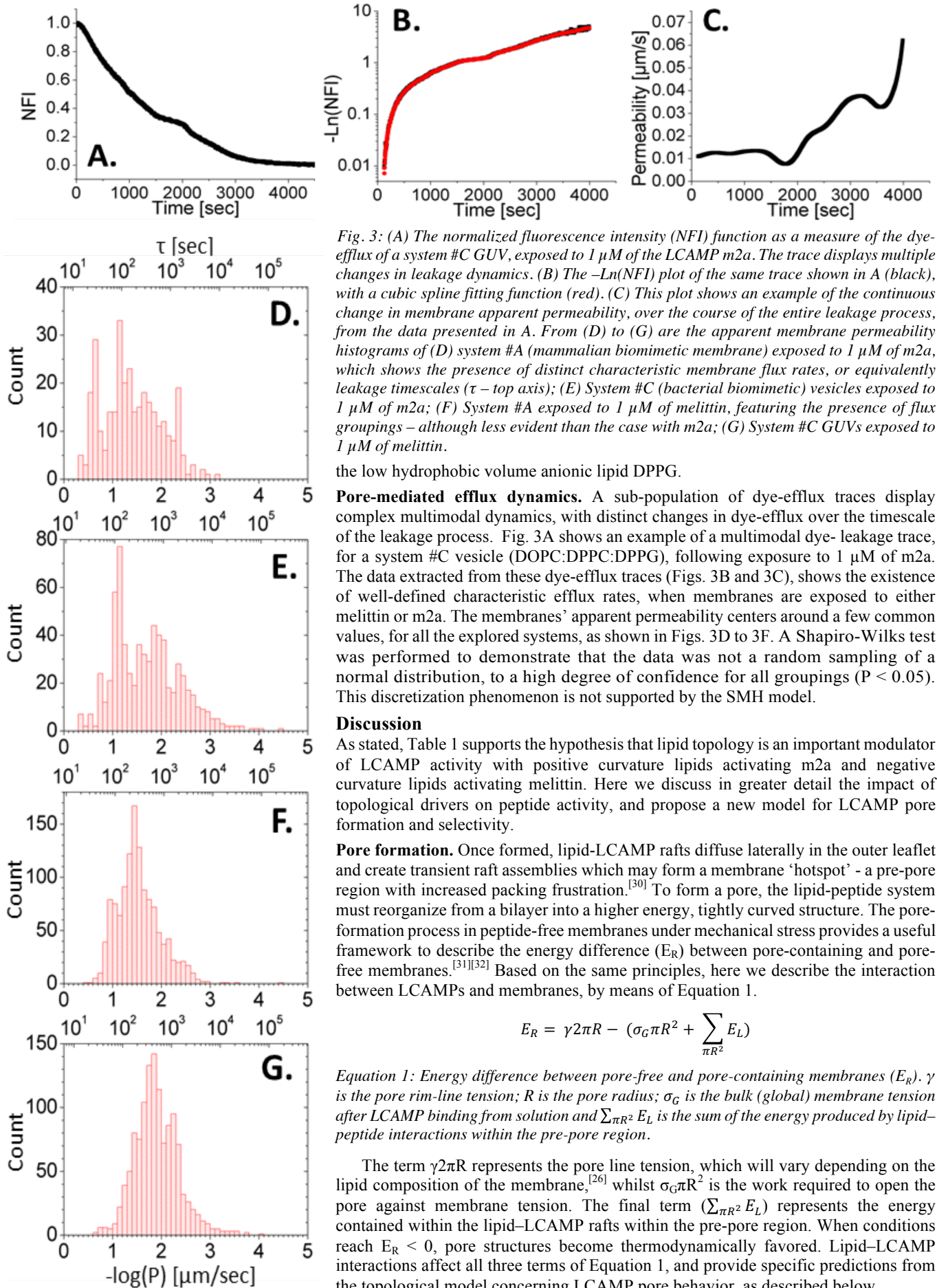


Fig. 3: (A) The normalized fluorescence intensity (NFI) function as a measure of the dye-efflux of a system #C GUV, exposed to 1 μM of the LCAMP m2a. The trace displays multiple changes in leakage dynamics. (B) The $-\ln(NFI)$ plot of the same trace shown in A (black), with a cubic spline fitting function (red). (C) This plot shows an example of the continuous change in membrane apparent permeability, over the course of the entire leakage process, from the data presented in A. From (D) to (G) are the apparent membrane permeability histograms of (D) system #A (mammalian biomimetic membrane) exposed to 1 μM of m2a, which shows the presence of distinct characteristic membrane flux rates, or equivalently leakage timescales (τ - top axis); (E) System #C (bacterial biomimetic) vesicles exposed to 1 μM of m2a; (F) System #A exposed to 1 μM of melittin, featuring the presence of flux groupings - although less evident than the case with m2a; (G) System #C GUVs exposed to 1 μM of melittin.

the low hydrophobic volume anionic lipid DPPG.

Pore-mediated efflux dynamics. A sub-population of dye-efflux traces display complex multimodal dynamics, with distinct changes in dye-efflux over the timescale of the leakage process. Fig. 3A shows an example of a multimodal dye-leakage trace, for a system #C vesicle (DOPC:DPPC:DPPG), following exposure to 1 μM of m2a. The data extracted from these dye-efflux traces (Figs. 3B and 3C), shows the existence of well-defined characteristic efflux rates, when membranes are exposed to either melittin or m2a. The membranes' apparent permeability centers around a few common values, for all the explored systems, as shown in Figs. 3D to 3F. A Shapiro-Wilks test was performed to demonstrate that the data was not a random sampling of a normal distribution, to a high degree of confidence for all groupings ($P < 0.05$). This discretization phenomenon is not supported by the SMH model.

Discussion

As stated, Table 1 supports the hypothesis that lipid topology is an important modulator of LCAMP activity with positive curvature lipids activating m2a and negative curvature lipids activating melittin. Here we discuss in greater detail the impact of topological drivers on peptide activity, and propose a new model for LCAMP pore formation and selectivity.

Pore formation. Once formed, lipid-LCAMP rafts diffuse laterally in the outer leaflet and create transient raft assemblies which may form a membrane 'hotspot' - a pre-pore region with increased packing frustration.^[30] To form a pore, the lipid-peptide system must reorganize from a bilayer into a higher energy, tightly curved structure. The pore-formation process in peptide-free membranes under mechanical stress provides a useful framework to describe the energy difference (E_R) between pore-containing and pore-free membranes.^{[31][32]} Based on the same principles, here we describe the interaction between LCAMPs and membranes, by means of Equation 1.

$$E_R = \gamma 2\pi R - (\sigma_G \pi R^2 + \sum_{\pi R^2} E_L)$$

Equation 1: Energy difference between pore-free and pore-containing membranes (E_R). γ is the pore rim-line tension; R is the pore radius; σ_G is the bulk (global) membrane tension after LCAMP binding from solution and $\sum_{\pi R^2} E_L$ is the sum of the energy produced by lipid-peptide interactions within the pre-pore region.

The term $\gamma 2\pi R$ represents the pore line tension, which will vary depending on the lipid composition of the membrane,^[26] whilst $\sigma_G \pi R^2$ is the work required to open the pore against membrane tension. The final term ($\sum_{\pi R^2} E_L$) represents the energy contained within the lipid-LCAMP rafts within the pre-pore region. When conditions reach $E_R < 0$, pore structures become thermodynamically favored. Lipid-LCAMP interactions affect all three terms of Equation 1, and provide specific predictions from the topological model concerning LCAMP pore behavior, as described below.

Pore rim-line tension ($\gamma 2\pi R$). Toroidal pores possess a tightly positively curved leaflet-fold structure where the inner and outer membrane leaflets bend into one another. Lipid curvature has been shown to stabilize, and/or induce nanoscale membrane curvature, reducing lipid packing frustration.^[26]

The sterically bulky amino acid residues, phenylalanine and tryptophan are key mediators of LCAMP activity although their precise role during pore formation remains unknown.^[7] Within the topological model, we propose that phenylalanine and tryptophan act as positionally flexible membrane topology wedges that are able to shift position within the membrane and manipulate the topography of the surrounding lipids. The positioning of one of these sterically bulky amino acids within the interfacial area of the outer leaflet increases the positive curvature of the adjacent lipids and favors pore formation through the stabilization of the leaflet fold structure (i.e. low γ value). Both phenylalanine and tryptophan residues are known to perform similar gating functions (shifting position within the membrane from the hydrophobic core to the interfacial region) for several transmembrane receptor proteins.^[33]

This process can be evaluated using the packing parameter (S), a metric which links lipid geometrical properties with their preferred supramolecular packing organization in aqueous environments.^[34] This measure is defined as $S = V/(a \times l)$, where V is the hydrocarbon volume, a is the headgroup area and l is the hydrocarbon chain length. Fig. 4 demonstrates this concept for m2a using three lipids in our dye-leakage experiments (i.e. DOPE, DPPC and DOPC). The new packing parameter, S^* , is calculated by adding the area of the main steric component of a phenylalanine residue (a benzene ring with a cross-sectional area of 40 \AA^2 ^[28]) to the headgroup area, a .

The conical non-bilayer lipid DOPE has a native S value of 1.41, forming inverse hexagonal phases in aqueous solution.^[34] When the headgroup area is occupied by the phenylalanine residues of m2a, the S value drops to 0.8, predictive of a bilayer system ($1.20 > S > 0.74$ is the requirement for stable bilayer formation^[35]). The cylindrical DOPC, and the inverse-conical DPPC, possess native S values indicative of bilayer structures.

In these cases, m2a forces S^* values below the bilayer threshold into geometries preferring hexagonal phase structures ($0.30 < S < 0.74$).^[35] This packing change is of particular interest, due to the similarities between the lipid packing of hexagonal-phases and idealized toroidal pore structures (see Fig. S10).

Given that pore formation is linked to peptide insertion parallel to the membrane normal, it is likely that the lipids along the helical face form the curved leaflet fold structure.^{[7][8]} LCAMPs that associate with positive curvature lipids along their helical face produce low γ values, favoring pore formation. Whereas, in systems where the peptide associates with either neutral or negatively curved lipids, higher γ values are produced, and consequently pore formation is decreased.

Work to open a pore ($\sigma_G \pi R^2$). This term is modified from previous work,^{[31][32]} by making the membrane tension sensitive to LCAMP binding. During the continuous exposure of a vesicle to LCAMPs within the microfluidic device, peptides constantly bind to the outer leaflet, with the consequence of thinning and weakening the membrane,^[9] i.e. σ_G continuously decreases with time, in proportion to the amount of membrane-bound LCAMP. Melittin inserts deep into the bilayer and results in a greater leaflet area asymmetry per peptide monomer than m2a,^{[8][20]} providing a higher contribution towards σ_G , and hence an increased activity. Moreover, the topological model predicts that pore formation should be dependent on vesicle size, due to the inverse-scaling of membrane tension with vesicle radius,^[36] which will alter σ_G . Consequently, a prediction of the topological model is that pores in small GUVs are harder to open than those in large GUVs, as they require greater work to open against their increased membrane tension. This is a marked departure from the established SMH model, which does not comment on vesicle size.

Lipid-peptide interaction energy (E_L). LCAMPs surrounded by lipids with matching curvature properties will increase raft packing frustration,^[37] and generate high E_L . Within anionic (i.e. bacterial) membranes, these high-energy interactions can be forced via electrostatics.^[12] The topological model proposes that for m2a inverse-conical anionic lipids

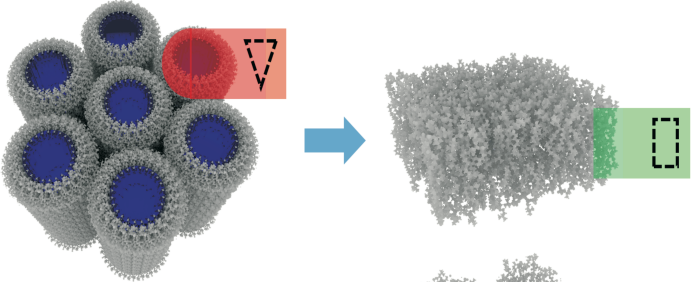
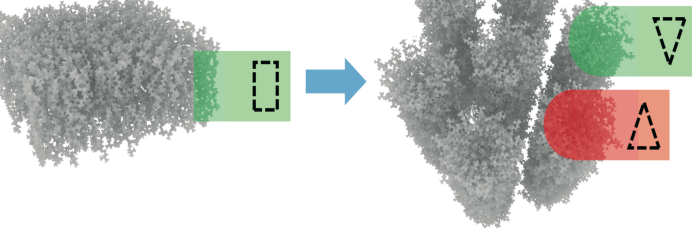
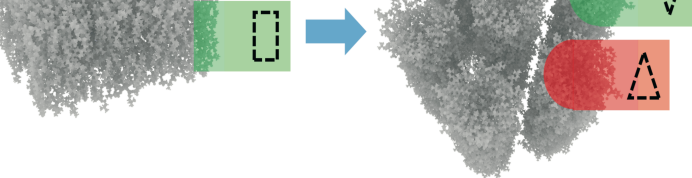
Lipid	S	Packing	F and W induced packing change	Packing*	S*
DOPE	1.41	HII		Bilayer	0.80
DOPC	1.08	Bilayer		HI	0.68
DPPC	0.78	Bilayer		HI	0.53

Fig. 4: The effect of F and W residues on the native packing parameters (S) and supramolecular packing arrangements of the lipids DOPE, DOPC and DPPC. The new packing parameter (S^*) and packing arrangement (packing*), after increasing the lipid headgroup area by the phenylalanine sidechains of m2a. DOPE changes from reverse-hexagonal phase (HII), to bilayer packing, and DOPC and DPPC change from bilayer to hexagonal phase (HI) packing. Values for calculations taken from [18][19][20][25][35][38].

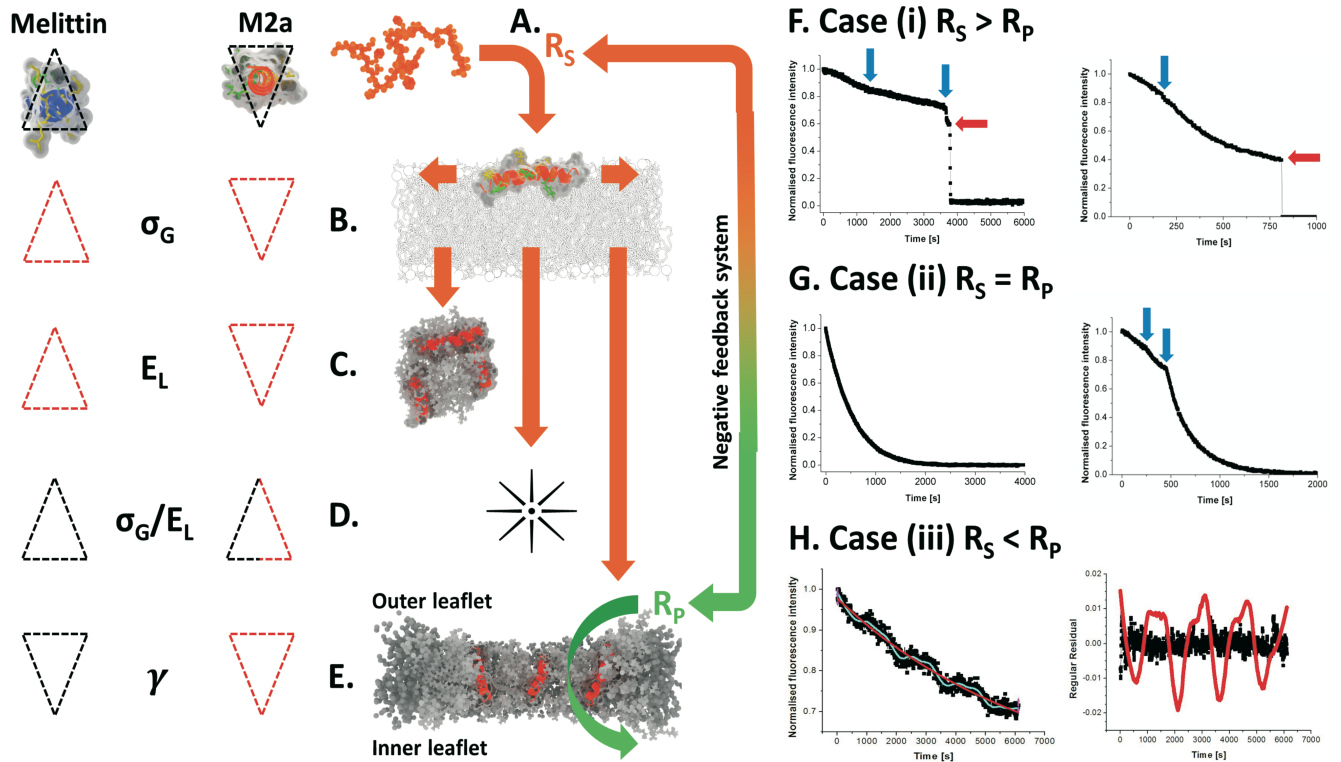


Fig. 5: The topological model proposes that lipid-peptide shape and charge interactions govern the behavior of LCAMPs, 5B to 5E show the specific lipid clustering and geometries responsible for individual PIEs, with lipid geometry shown using block shapes, and clustering lipids given a red outline. The terms of Equation (1) associated with each PIE are also shown. (A) Peptide binds to the outer leaflet, generating internal membrane strain (σ_G), which controls overall activity (B). Both peptides are more active when clustered with lipids matching their own curvature strain; melittin with conical lipids and m2a with inverse-conical lipids. (C) Clustering with lipids matching peptide curvature also governs the carpet mechanism, by generating high E_L values, and stabilizing the high curvature lipid-peptide micelles produced. (D) Bursting events for melittin occur when the membrane contains non-clustering conical lipids, which will generate high E_L raft assemblies that cannot react via pore formation (high γ), instead they cause complete vesicle failure. For m2a both clustering and non-clustering conical lipids cause bursting. (E) Melittin generates pore activity (low γ) when inverse-conical lipids associate with its helical face, while m2a generates pores when clustered with inverse-conical lipids. Open pores allow interleaflet material transfer, lowering σ_G , and generating a negative feedback system between the rate of LCAMP binding from solution (R_S), and the rate of material flow through open pores (R_P), with three possible cases: (i) $R_S > R_P$, shown in (F), there is a continuous increase in σ_G , causing pore opening (blue arrows) until the membrane failure point is reached and the vesicle bursts (red arrows). Examples are shown for System #A exposed to m2a (left) and for System #C for melittin (right), which displays complex leakage dynamics, as several pores open (blue arrows) prior to a stable leak being established; (ii) $R_S = R_P$, resulting in a stable leak (G), shown for system #C for m2a (left) and melittin (right); (iii) $R_P > R_S$, decreasing σ_G , and favoring pore closure. This renders $R_S > R_P$, increasing σ_G , and reinitiating pore-formation. This results in pore opening and closing cycles. (H, left) shows a pore-cycling leakage trace (system #F, m2a), with its smoothed average (light blue) and fitted single exponential decay curve (red). (H, right) The residual between the two curves shown in H, left (red), compared to the residual for a stable case (ii) leak (black). The residual shows dynamic cycling between at least two different leakage rates, with intervals between the minima of 1517, 1512 and 1611 s. Consistent cycle spacing is due to the constant R_S within the microfluidic device.

(e.g. DPPG) can be brought into close proximity to the peptides three phenylalanine (F) residues, because of their close spatial relationship with the peptides cationic lysine (K) residues (see Fig. 2); specifically K4 and F5; K10/11 and F12; K14 and F16. These large headgroup lipids will compete for interfacial area with the F residues of m2a, generating increased lipid-peptide packing frustration and increasing E_L . Conversely, melittin will generate large E_L values when surrounded by conical lipids, owing to its induction of negative curvature.

Extended LCAMP model

Here, based on our experimental results, we summarize our proposed topological model (Figs. 5A to 5E), which adds both explanatory and predictive power to the SMH model (Fig. 6). LCAMP behavior can be understood by means of simple concepts, namely lipid-peptide charge and topological interactions. The process is driven by the accumulation of strain within the target membrane through the occupation of outer

leaflet volume by the LCAMP binding from solution. The precise nature of PIEs seen within a membrane is controlled by the charge and topological interactions occurring within the lipid-peptide rafts.

Overall activity is controlled by clustering with lipids that match the peptides own curvature - negative (conical) and positive (inverse-conical) curvatures for melittin and m2a respectively (Fig. 5B), that generate high σ_G . The carpet mechanism is promoted by clustering with similar lipids, at the c-terminus of melittin, and along the helical face of m2a (Fig. 5C), causing high E_L . The combination of peptide and lipid curvature can stabilize the tightly curved lipid-peptide micelles produced by the carpet mechanism. Bursting is favored by conical lipids for both peptides, although melittin associating with high hydrophobic volume clustering lipids tends to react via the carpet mechanism, while m2a show sensitivity to both clustering and non-clustering conical lipids (Fig. 5D). The data

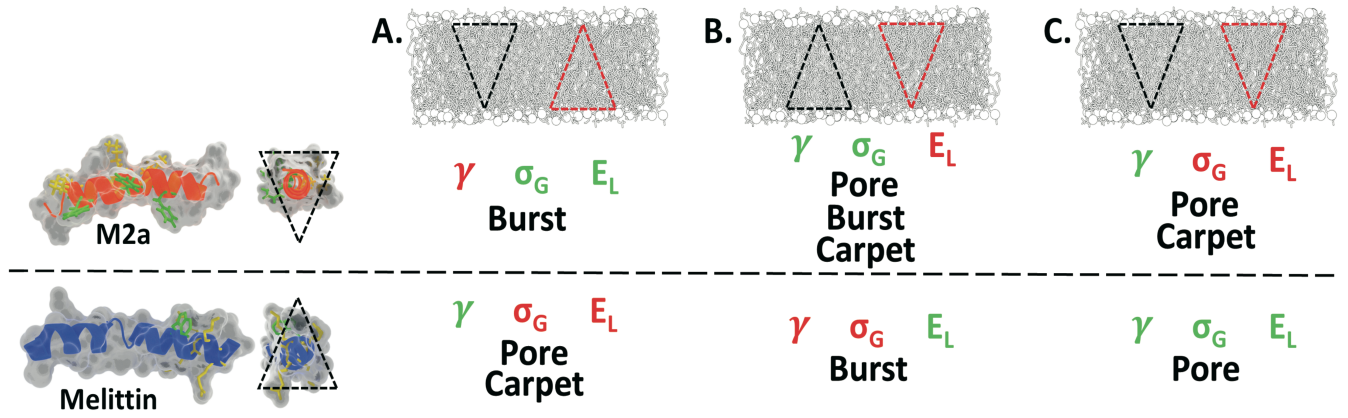


Fig. 6: Predictions for LCAMP behavior within new membranes, based on the lipid-peptide topological interactions, and their effects on the terms of equation one (γ : pore rim line tension; σ_G : membrane tension and E_L : lipid-peptide interaction energy). The lipid topology of the membrane systems is indicated by block shapes, with lipids having a clustering mechanism given a red outline. Within (A), m2a generates high γ values (red), but low σ_G and E_L (green) through clustering with conical lipids along its helical face. Pore mechanism is suppressed via inefficient leaflet fold packing, while carpet mechanism is suppressed by nullification of the peptides positive curvature. M2a will therefore react via bursting. Melittin clusters the conical lipids at its c-terminus, and associate with the inverse-conical lipids along its helical face. This generates low γ , combined with high E_L at the c-terminus, and will respond via both pore (low γ) and carpet mechanisms (high E_L). (B) In this membrane, m2a clusters inverse-conical lipids at its helical face, generating low γ and high E_L , which together with the presence of conical non-bilayer lipids, allows the peptide to produce all three PIEs. Melittin generates higher γ and lower E_L , and primarily react via bursting. (C) M2a produces low γ and high E_L , through clustering with inverse-conical lipids along its helical face. This will generate pore and carpet mechanisms. Melittin generates low γ and E_L , and will be forced to react mainly via bursting.

suggest that bursting occurs when the LCAMPs associate with lipids that disfavor other PIEs, such as clustering with high hydrophobic volume lipids, which disfavor efficient leaflet fold packing, or with lipids opposing the peptides own curvature induction, suppressing the carpet mechanism. Pore-formation is favored via the association of inverse-conical positive curvature lipids for both melittin and m2a (Fig. 5E). A negative feedback system, between LCAMPs binding from solution and lipid-peptide transfer between leaflets through open pores, governs peptide pore-formation (Figs 5F to 5H).

Model predictions. Using the patterns in lipid-peptide topological interactions and their effects on the terms of Equation 1, it is possible to make general predictions concerning the PIE activity of LCAMPs within new membrane systems of defined topology and charge (Figs. 6A to 6C)

Negative feedback and toroidal pores. Pore leakage dynamics can be explained by the inclusion of a negative feedback system within the topological model (Figs. 5F to 5H). Toroidal pores are dynamic structures facilitating lipid and peptide transfer between the membrane leaflets,^{[7][8][22]} which amounts to a membrane-relaxation process, reducing leaflet area asymmetry. Each pore opening renders subsequent pore openings less likely, creating negative feedback between the rate of LCAMP binding from solution (R_S), the flow of the lipid-LCAMP material through open pores (R_P) and the energy needed to open a pore structure (σ_G). This framework leads to three possible outcomes, all of which are consistent with the leakage dynamics recorded for m2a and melittin (Fig. 5F to 5H):

(i) $R_S < R_P$: Leaflet asymmetry continually increases, allowing raft assemblies of lower total E_L to create pores (Fig. 5F). A cascade of pore formation occurs until the membrane failure is reached and the GUV bursts.

(ii) $R_S = R_P$: When the rates are in equilibrium during the leakage process (Fig. 5G). Initially R_S is higher than R_P and, as membrane tension increases, this causes pore formation and

increases R_P . When R_S and R_P are equal, a stable leakage state can occur.

(iii) $R_P > R_S$: Loss of outer leaflet volume decreases the area asymmetry between the outer and inner leaflets, decreasing membrane tension and causing pore closure, until $R_S > R_P$ and pore activity resumes. The negative feedback loop leads to cycles of high and low pore activity, as membrane tension repeatedly crosses the energy threshold required for lipid-LCAMP rafts to form pores (Fig. 5H).

We propose that this negative feedback explains the discretizing of LCAMP pore leakage behavior observed in Fig. 3, where leakage traces arrange in groups with similar dynamics, which are controlled by the pore size and number within the membrane (i.e. by their apparent permeability). We next apply the model to the selectivity mechanism of LCAMPs, between mammalian and bacterial cells.

Implications for selectivity. Deciphering and controlling selectivity is a key consideration in the development of antimicrobial agents and our topological model provides a powerful tool to understand this process. To succeed as antimicrobial agents, LCAMPs must form pores in bacterial membranes (i.e. render $E_R < 0$), while leaving mammalian membranes intact ($E_R > 0$). Using our lipid systems as examples, we explore how the characteristic electrostatic and topological differences between bacterial and mammalian membranes affect the terms in Equation 1, yielding important considerations for peptide selectivity.

The opposing charge and topological characters of the non-selective melittin, and the selective m2a, mean that within identical membranes, they can form rafts enriched with different lipids (Fig. 2). The clustering of melittin's charged and sterically bulky residues at one end of the helix leaves the helical face free to interact with zwitterionic membrane components, making melittin more sensitive to zwitterionic lipid topology than m2a, whose cationic residues are distributed along its helical length.

Bacterial outer membrane leaflets contain anionic lipids, many of which have large headgroups and inverse-conical geometries.^{[12][19]} Electrostatic interactions can force these lipids into close contact with the helical face of m2a, favoring pore formation through efficient pore leaflet fold packing (i.e. low γ), and forcing unfavorable high E_L topological interactions. For example, in system #C (DOPC:DPPC:DPPG) m2a is an efficient pore former, returning the highest relative ratio of pore activity (78%). Bacterial membranes also contain a large proportion of conical non-bilayer lipids like DOPE,^[19] similar to Fig. 6B. These lipids induce membrane packing frustration into the bilayer. This lowers the barrier to pore formation; i.e. lower contribution from σ_G to render $E_R < 0$. Notably, pore formation by m2a in system #F occurred faster than in any other membrane system tested (Table S3), although the reduced positive curvature lipid content compared to system #C, produced lower relative pore formation (54%). The supplementary information contains a more detailed discussion of the implications of the model, for the timings of PIE initiation, for membrane systems #A to #G.

Mammalian cells maintain zwitterionic outer membrane leaflets, composed of bilayer lipids with large headgroups like phosphatidylcholine, and contain cholesterol,^[18] a membrane component completely absent from bacteria (similar to Fig. 6A). Within mammalian membranes m2a is free from forced electrostatic interactions, and can associate with lipids that minimize its raft energy (Fig. 2). M2a pore-activity is notably suppressed in the mammalian biomimetic membrane (system #A), where the peptide is expected to form cholesterol enriched rafts through π -stacking interactions with its phenylalanine residues.^{[28][29]} This puts a negative curvature, high hydrophobic volume lipid into association with the peptide, which will not efficiently pack the pores leaflet fold (i.e. high γ), both lowering raft energy (i.e. low E_L) and disfavoring pore formation. M2a was generally less active than melittin, however in membranes with specific charge and topologies it is capable of fast and efficient pore formation.

Conclusions

High-throughput analysis of dye-leakage experiments of GUVs with different lipid compositions has enabled the in-depth study of the membrane-disrupting properties of LCAMPs. This has allowed us to propose the presence of a negative feedback system, between membrane strain (σ_G) and pore opening, that can be used to describe pore behavior. By using steric and electrostatic interactions as primary considerations, we have developed a model for LCAMP behavior, that provides a predictive mechanism for activity and selectivity. The model has potential application in the rationale design of new therapeutics, which are urgently required to combat the rapid spread of drug-resistant bacterial strains. By using the proposed models framework, LCAMPs can be designed to generate efficiently packed pores (low γ), together with high-leaflet area asymmetry (σ_G) and lipid-LCAMP interaction energy (E_L) within a variety of membranes, providing the opportunity of tailoring peptide activity to specific bacterial membranes. We propose that lipids must be considered involved participants in the membrane-disruption caused by LCAMPs, instead of being merely passive participants in the process.

Materials and Methods

The materials and methods are described in detail within the supplementary information. Briefly, GUVs were formed by *in-*

situ electroformation within the microfluidic device from seven different lipid compositions (#A to #G), of varying topology and charge (Table S1). System #A is based on a typical mammalian membrane composition, and systems #B to #G are based on an *E.coli* membrane, which is dominated by phosphatidylethanolamine (PE) and phosphoglycerol (PG) lipid species.^[38] Membrane topography was varied by changing the proportions of 16:0 and 18:1 fatty acid chains of the PG species, and exchanging the PE headgroup for the larger PC headgroup.

A fluorescent marker (AlexaFluor488-3k dextran) was incorporated within the GUVs, which were captured within a microfabricated trap array. Trapped GUVs were exposed to either a non-selective LCAMP (melittin) or a selective LCAMP (m2a) using microfluidic dispensation to precisely control both the duration of exposure and the final peptide concentration. GUVs were imaged during LCAMP exposure using confocal microscopy (Zeiss LSM 510 Live) at a data capture frequency of 0.25 fps.^[23] Activity was defined by the proportion of GUVs showing PIEs; either pore-mediated leakage, bursting or carpet mechanism (defined as shown in Figs. S4 to S8). Data was collated into characteristic profiles, describing the frequency (%) of each of the three behaviors, within the seven lipid compositions (#A to #G).

Acknowledgements

Research was funded by the EPSRC (DTC: EP/F500424/1, Proxomics: EP/I017887/1 and Frontiers: EP/K038885/1). JC acknowledges support from an EPSRC Personal Fellowship (EP/K027611/1) and an ERC Advanced Grant Bio-Phononics. MT acknowledges the Royal Academy of Engineering/EPSRC Fellowship (10216/101). JR acknowledges the University of Glasgow Lord Kelvin and Adam Smith Research Fellowship. The authors thank Dr. Alasdair Clark (University of Glasgow, UK) for scanning electron microscopy and the James Watt Nanofabrication Centre (University of Glasgow, UK) for help with device fabrication.

References

- [1] Cohen ML (2000) *Changing patterns of infectious disease*. Nature. **406**: pages 762 – 767.
- [2] Centers for Disease Control and Prevention Threat report: Antibiotic resistance threats in the United States, 2013.
- [3] Davies J (2006) *Bacteria on the rampage*. Nature. **383**: pages 219 – 220.
- [4] Walsh C (2000) *Molecular mechanisms that confer antibiotic drug resistance*. Nature. **406**: pages 775 – 781.
- [5] Al-Ani I, Zimmermann S, Reichling J and Wink M (2015) *Pharmacological synergism of bee venom and melittin with antibiotics and plant secondary metabolites against multi-drug resistant microbial pathogens*. Phytomedicine, **22** (2) pages 245 – 255.
- [6] Zasloff M (2002) *Antimicrobial peptides of multicellular organisms*. Nature. **415**: pages 389 – 395.
- [7] Raghuraman H and Chattopadhyay A (2007) *Melittin: A membrane-active peptide with diverse functions*. Bioscience Reports. **27**: pages 189 – 223.
- [8] Matsuzaki K, Sugishita K, Harada M, Fujii N and Miyajima K (1997) *Interactions of an antimicrobial peptide, magainin 2, with outer and inner membranes of gram-negative bacteria*. Biochimica et Biophysica Acta. **1327**: pages 119 – 130.
- [9] Bechinger B and Lohner K (2006) *Detergent-like actions of linear amphipathic cationic antimicrobial peptides*. Biochimica et Biophysica Acta. **1758**: pages 1529 – 1539.
- [10] Haney EF and Hancock RE (2013) *Peptide design for antimicrobial and immunomodulatory applications*. Biopolymers, **100**, (6), pages 572 – 583.

- [11] Oren Z and Shai Y (1997) *Selective lysis of bacteria but not mammalian cells by diastereomers of melittin: structure-function study*. *Biochemistry*, **36**, pages 1826 – 1835.
- [12] Epand RF, Maloy WL, Ramamoorthy A and Epand RM (2010) *Probing the “charge cluster mechanism” in amphipathic cationic antimicrobial peptides*. *Biochemistry*, **49** (19): pages 4076 – 4084.
- [13] Dathe M, Wieprecht T, Nikolenko H and Bienert M (1997) *Hydrophobicity, hydrophobic moment and angle subtended by charged residues modulate antibacterial and haemolytic activity of amphipathic helical peptides*. *FEBS Letters*, **403**, (2), pages 208 – 212.
- [14] Dathe M and Wieprecht T (1999) *Structural features of helical antimicrobial peptides: their potential to modulate activity on model membranes and biological cells*. *Biochimica et Biophysica Acta (BBA) – Biomembranes*, **1462** (1 – 2): pages 71 – 87.
- [15] Shai Y (1999) *Mechanism of the binding, insertion and destabilization of phospholipid bilayer membranes by K-helical antimicrobial and cell non-selective membrane-lytic peptides*. *Biochimica et Biophysica Acta*, **1462**: pages 55 – 70.
- [16] Brogden KA (2005) *Antimicrobial peptides: Pore formers or metabolic inhibitors in bacteria?* *Nature Reviews Microbiology*, **3**: pages 238 – 250.
- [17] Yang L, Harroun TA, Weiss TM, Ding L and Huang HW (2001) *Barrel-stave model or toroidal model? A case study on melittin pores*. *Biophysical Journal*, **81**: pages 1475 – 1485.
- [18] van Meer G and de Kroon AIPM (2011) *Lipid map of the mammalian cell*. *Journal of Cell Science*, **124**: pages 5 – 8.
- [19] Silhavy TJ, Kahne D and Walker S (2010) *The bacterial cell envelope*. *Cold Spring Harbour Perspectives on Biology*, **2** (5): a000414
- [20] Batenburg AM, van Esch JH and de Kruijff B (1988) *Melittin-induced changes of macroscopic structure of phosphatidylethanolamines*. *Biochemistry*, **27** (7): pages 2324 – 2331.
- [21] Ladokhin AS, Selsted ME and White SH (1997) *Sizing membrane pores in lipid vesicles by leakage of coencapsulated markers*. *Biophysical Journal*, **72**: pages 1762 – 1766.
- [22] Matsuzaki K, Yoneyama S and Miyajima K (1997) *Pore formation and translocation of melittin*. *Biophysical Journal*, **73**: pages 831 – 838.
- [23] Paterson DJ, Reboud J, Wilson R, Tassieri M and Cooper JM (2014) *Integrating microfluidic generation, handling and analysis of biomimetic giant unilamellar vesicles*. *Lab on a Chip*, **14** (11): pages 1806 – 1810.
- [24] Hebbar S, Lee E, Manna M, Steinert S, Kumar GS, Wenk M, Wohland T and Kraut R (2008) *A fluorescent sphingolipid binding-domain peptide probe interacts with sphingolipids and cholesterol-dependent raft domains*. *Journal of Lipid Research*, **49** (5): pages 1077 – 1089.
- [25] Callan-Jones A, Sorre B and Bassereau P (2011) *Curvature-driven lipid sorting in biomembranes*. *Cold Spring Harbour Perspectives in Biology*, **3** (2): a004648.
- [26] Zimmerberg J and Koslov MM (2006) *How proteins produce cellular membrane curvature*. *Nature Reviews Molecular Cell Biology*, **7**: pages 9 – 19.
- [27] Almeida PF, Pokorny A and Hinderliter A (2005) *Thermodynamics of membrane domains*. *Biochimica et Biophysica Acta*, **1720**: pages 1 – 13.
- [28] Fantini J and Barrantes FJ (2013) *How cholesterol interacts with membrane proteins: an exploration of cholesterol-binding sites including CRAC, CARC, and tilted domains*. *Frontiers in Physiology*, **4** (31): pages 1 – 9.
- [29] Zhou X and Xu J (2012) *Free cholesterol induces higher β -sheet content in A β peptide oligomers by aromatic interaction with Phe19*. *PLoS ONE*, **7** (9): e46245. Doi: 10.1371/journal.pone.0046245.
- [30] Mahalka AK and Kinnunen PKJ (2009) *Binding of amphipathic α -helical antimicrobial peptides to lipid membranes: Lessons from temporins B and L*. *Biochimica et Biophysica Acta*, **1788** (8): pages 1600 – 1609.
- [31] Lee M-T, Chen F-Y and Huang HW (2004) *Energetics of pore formation induced by membrane active peptides*. *Biochemistry*, **43**: pages 3590 – 3599.
- [32] Leontiadou H, Mark, AE and Marrink SJ (2004) *Molecular dynamics simulations of hydrophilic pores in lipid bilayers*. *Biophysical Journal*, **86** (4): pages 2156 – 2164.
- [33] Kelkar DA and Chattopadhyay A (2006) *Membrane interfacial localization of aromatic amino acids and membrane protein function*. *Journal of Biosciences*, **31** (3)L pages 297 – 302.
- [34] Isrealachvili J, Mitchell J and Ninham B (1976) *Theory of self-assembly of hydrocarbon amphiphiles into micelles and bilayers*. *Journal of the Chemical Society, Faraday Transactions 2: Molecular and Chemical Physics*, **72**: pages 1525 – 1568.
- [35] Kumar VV (1991) *Complementary molecular shapes and the additivity of the packing parameter of lipids*. *Proceedings of the National Academy of Science USA*, **88**: pages 444 – 448.
- [36] Karatekhin E, Sandre O, Guitouni H, Borghi N, Puech PH and Brochard-Wyart F (2003) *Cascades of transient pores in giant vesicles: Line tension and transport*. *Biophysical Journal*, **84**: pages 1734 – 1749.
- [37] Schneggenburger PE, Beerlink A, Weinhausen B, Salditt T and Diederichsen U (2011) *Peptide model helices in lipid membranes: insertion, positioning, and lipid response on aggregation studied by X-ray scattering*. *Eur. Biophys. J.*, **40**, pages 417 – 436.
- [38] Oursel D, Loutelier-Bourhis C, Orange N, Chevalier S, Norris V and Lange CM (2007) *Lipid composition of membranes of Escherichia coli by liquid chromatography/tandem mass spectrometry using negative electrospray ionization*. *Rapid Communications in Mass Spectrometry*, **21** (11): pages 1721 – 1728.
- [39] Angelova M, Soleau S, Meleard P, Faucon JF and Bothorel P (1992) *Preparation of giant vesicles by external A.C. electric fields. Kinetics and applications*. *Progress in Colloid and Polymer Science*, **89**: pages 127 – 131.
- [40] Estes DJ and Mayer M (2005) *Giant liposomes in physiological buffer using electroformation in a flow chamber*. *Biochimica et Biophysica Acta (BBA)*, **17** (2): pages 152 – 158.
- [41] Wheaton SA, Lakshmanan A and Almeida PF (2013) *Statistical analysis of peptide-induced graded and all-or-none fluxes in giant vesicles*. *Biophysical Journal*, **105**: pages 432 – 443.
- [42] Durrant JD and Amaro RE (2014) *Lipidwrapper: An algorithm for generating large-scale membrane models of arbitrary geometry*. *PLoS Comput. Biol.*, **10**, (7), e1003720.
- [43] Meng Y, Shukla D, Pande VS and Roux B (2016) *Transition path theory analysis of c-Src kinase activation*. **113**, pages 9193 – 9198.
- [44] Versace RE and Lazaridis T (2015) *Modelling protein-micelle systems in implicit water*. *J. Phys. Chem. B.*, **119**, pages 8037 – 8047.